Energy Storage Materials 16 (2019) 91–96

Contents lists available at ScienceDirect

Energy Storage Materials

journal homepage: www.elsevier.com/locate/ensm

Particle based method and X-ray computed tomography for pore-scale flow characterization in VRFB electrodes

Dario Maggiolo[a,*], Filippo Zanini[b], Francesco Picano[c], Andrea Trovò[c], Simone Carmignato[b], Massimo Guarnieri[c]

[a] Department of Mechanics and Maritime Sciences, Chalmers University of Technology, Hörsalsvägen 7A, 41296 Göteborg, Sweden
[b] Department of Management and Engineering, University of Padova, Stradella San Nicola 3, 36100, Vicenza, Italy
[c] Department of Industrial Engineering, University of Padova, Via Gradenigo 6/A, 35131 Padua, Italy

ARTICLE INFO

Keywords:
Redox flow battery
Lattice-Boltzmann
Lagrangian particle tracking
X-ray computed tomography
Porous electrode

ABSTRACT

Porous electrodes are pivotal components of Vanadium Redox Flow Batteries, which influence the power density, pressure drop losses, activation overpotentials, limit current density, bulk and contact resistance, and ohmic losses. The quantification of the fluid-mechanic efficiency of porous electrodes based on their real geometry is a useful measure, as it primarily affects the mass transport losses and the overall battery performances. Although several studies, both numerical and experimental, have been devoted to the electrode enhancement, most analyses are carried out under the simplifying assumption of linear, macrohomogeneous and isotropic behavior of the fluid mechanics in the porous material. We present an original approach built on the Lattice-Boltzmann Method and Lagrange Particle Tracking that makes use of pore-scale accurate geometrical data provided by X-ray computed tomography with the aim of studying the dispersion and reaction rates of liquid electrolyte reactants in the flow battery porous electrode. Following this methodology, we compare the fluid-dynamic performances provided by a commonly used carbon felt and an unconventional material, that is, a carbon vitrified foam. Surprisingly, results unveil the possibility of achieving higher fluid-mechanic efficiencies with the foam electrode, whose intrinsic microstructure promotes higher reaction rate.

1. Introduction

Stationary energy storage has a key role in the expansion of decarbonized renewable energy sources, which are typically intermittent, and of smart grids provided with distributed energy-management capability. Energy storage systems are required to provide a variety of services with response times ranging from milliseconds to minutes and discharge duration ranging from minutes to several hours. Seasonal storage implies the capability of preserving energy storage over some months with limited self-discharge. Electrochemical Energy Storage is the solution of choice for fast power quality services, for small power/energy ratings, and for the general distributed exploitation that is required in smart grids. In fact it has grown fast in last years, its rated power passing from 0.1 GW as of 2007 to 1, 7 GW as of 2017 [1]. Even if Lithium-ion batteries are presently the most successful technology in the stationary market, after gaining a dominant position in the portable electronics and electric mobility sectors, beyond-lithium forecasts indicate that Redox Flow Batteries (RFBs) will have a major boost for stationary energy storage in the next future [2].

They feature a unique combination of advantages including: very fast response times, of the order of millisecond in stand-by mode; independent sizing of power and energy allowing for discharges long at will; a single reversible device performing energy storage and delivery; good round-trip efficiency; and virtually no self-discharge in off-mode. The Vanadium RFB (VRFB), that is the only widely marketed version at present, presents extremely long calendar and cycle lives, in excess of 20 years and 20,000 cycles, respectively, thanks to the use of the same metal in the two electrodes, that prevents cross-contamination and limits membrane aging. However, VRFBs also suffer from some drawbacks which limit their present market competitiveness, notably low energy density, due to limited solubility of the electrolyte in the sulphuric acid solution, and low power density, related to the limited

* Corresponding author.
E-mail addresses: maggiolo@chalmers.se (D. Maggiolo), Bfilippo.zanini@unipd.it (F. Zanini), cfrancesco.picano@unipd.it (F. Picano), dandrea.trovo@unipd.it (A. Trovò), esimone.carmignato@unipd.it (S. Carmignato), massimo.guarnieri@unipd.it (M. Guarnieri).

https://doi.org/10.1016/j.ensm.2018.04.021
Received 4 January 2018; Received in revised form 17 April 2018; Accepted 18 April 2018
Available online 24 April 2018

current density generated in the electrodes. Industrial-size cells have average current densities much lower than top values obtained in experimental small-size single-cell devices.

1.1. Mass transport losses in VRFB

The main sources of losses in a VRFBs are electrochemical, ohmic and concentration polarizations. While the former two are significant at low current densities, the latter mainly affect the battery behavior at high current densities. Concentration polarization occurs since in the electrolyte diffusive mass transport ($\mathcal{D}_m \sim 10^{-3}$ mm^2/s) is much slower slower than momentum diffusivity ($\nu \sim 1$ mm^2/s) and the fluid-mechanic efficiency of the system is poor. The too-slow mass transport of reactants limits the battery current density. A proper design of the cell and porous microstructure can mitigate this technological issue. This work focuses on this important issue.

Two arrangements for distributing the solutions inside the electrodes are typically considered: the flow-through and the flow-by design. The former requires thick, highly porous and little compressed electrodes characterized by relatively high bulk and contact resistances [3]. Instead, in the latter, liquid electrolytes are distributed into thin paper electrodes from channels engraved in thicker current collectors which provide better contact resistance. Nevertheless, this solution typically shows poor electrochemical behavior and smaller active surface areas [4]. An extensive literature deals with flow field design documenting the much work done in order to increase the uniformity of the electrolyte distribution along the cell area, making use of alternative design concepts [5–7]. Typically, the aforementioned analyses adopt the macrohomogeneous porous electrode approach. In this view, permeability and diffusion in the porous electrode are modeled through homogeneous equivalent parameters, e.g. by means of the Bruggeman approximation. [8].

Even though such efforts have been rewarded with improved performances, few studies focus on the phenomena occurring at microscopic scales which are at the base of the VRFB fluid-dynamic efficiency. X-ray computed tomography (CT) was early used for investigating VRFB electrodes by Qiu et al. [9,10], who proposed a methodology for modeling the transport mechanisms of species and charge in the VRFB at the pore scale. They used CT data as geometry input for the flow field of electrolyte that was modeled using the Lattice-Boltzmann Method (LBM). Transport of species and charge was formulated by means of the finite volume method (FVM) with the Butler-Volmer equations which model the species and charges coupling at the active surface sites. They obtained local concentration, overpotentials, current density and cell voltage, finding a cell voltage increase with increasing electrolyte flow rate due to decreasing concentration gradients. Trogadas et al. [11] combined CT of voltage-cycled graphite felts, scanning electron microscopy (SEM), and X-ray photoelectron spectroscopy (XPS) to capture the changes in felt structure and properties such as porosity, characteristic tortuosity and volume specific surface area, during operation. Jervis et al. [12] designed a miniature flow cell that allowed the use of CT to study carbon felt materials *in situ* and *operando*, in both lab-based and synchrotron CT. Their bespoke cell can be used to observe felt fibers, electrolyte and pore phases, enabling non-destructive characterization of an array of microstructural parameters during the operation.

However, to the best of our knowledge such diagnostic techniques where not yet used to compare effects and performances of different porous microstructures of real VRFB electrodes. In this paper we present an original approach that resorts to the Lattice-Boltzmann Method and Lagrange Particle Tracking and makes use of material geometry data obtained using a X-ray CT system to investigate the dispersion and reaction rates induced by different microstructure of the VRFB porous electrode. Through this technique we obtain a pore-scale non-homogeneous anisotropic analysis and parametrization of the flow filed inside two different materials for VRFB electrodes: a commonly used carbon felt and a carbon vitrified foam. The surprising results of this analysis show that the foam microstructure induces higher dispersion and reaction rates which in turn can increase VRFB fluid-mechanic performances.

2. Methodology

The fluid-dynamic performance of porous electrodes strongly depends on the microstructure of the media. From an experimental point of view only global properties can be measured. Local flow features, e.g. electrolyte dispersion or velocity, are very difficult to measure since optical accesses through porous electrodes are difficult to use without altering the local geometry. Recent computational methods and resources open new perspectives in the detailed analysis of these devices. The procedure we propose aims to evaluate the performance of different porous electrode microstructures mixing state-of-the-art metrology and numerical simulation techniques.

In particular, we use X-ray CT to reconstruct the real microstructure of porous media, a Lattice-Boltzmann flow solver to simulate the microscopic flow behavior through the pores of the electrodes and a Lagrangian Particle Tracking method to evolve the electrolyte dispersion and reaction through the medium. The synergy of all these different competences is used to evaluate electrode performance at fixed pump power in terms of electrolyte dispersion and reaction rate in the limit of fast chemistry. The main advantage of the proposed methodology is a detailed characterization from microscopic to macroscopic properties of the media which is presently unfeasible with a pure experimental approach. In fact, by means of the present methodology, we are able to obtain: (i) a geometrical reconstruction of the electrode with high resolution that allows to capture the typical small length scale of the pores (the voxel size $\sim 5\,\mu m$ is one/two orders of magnitude smaller than the mean pore size diameter in VRFB electrodes, see e.g. [13]) and (ii) a full characterization of the electrolyte flow field at the same length scale (the LBM computational cell size corresponds to the X-ray CT voxel size). Each technique forming the procedure is described in one of the following sections.

2.1. X-ray computed tomography

Dispersion and reaction mechanisms in porous and/or fibrous media are connected to the specific material properties, including the internal configuration (i.e. spatial disposition and volume of interconnected pores and fiber orientation). In order to fully understand how such mechanisms can affect the performances of real electrodes of flow batteries, an analysis of the internal material characteristics should be conducted. However, analyzing non-accessible features is impossible with conventional methods. For example, internal porosity is commonly investigated by the Archimedes method, which measures only the percentage content of pores, or by optical analyses, which require destructive operations and are limited to few cut-sections [14]. Also the fiber orientation can be studied using destructive techniques from the geometry of elliptical cross-sectional shape of fibers, in correspondence to specific consequential cut-planes of the specimen [15].

An advanced technology capable of overcoming the limitations of the above mentioned methods is X-ray CT, which enables non-destructive analyses of both external and internal features [16,17]. In particular, material porosity can be evaluated in terms of spatial distribution, size and morphology [14] and the fiber orientation can be successfully assessed from CT data throughout the entire part [18]. Another advantage of CT is that soft and fragile parts, as the samples investigated in this paper, can be scanned without risks of damages or deformations. Furthermore, CT systems specifically developed for coordinate metrology are currently available to perform accurate measurements [19]. Given these features, X-ray CT has been already used for characterizing porous electrodes [9,10] but it has been never used for investigating innovative materials.

Table 1
CT scanning parameters for two electrodes made of different materials: carbon felt (Sample 1) and carbon vitrified foam (Sample 2).

Parameter	*Felt*	*Foam*
Voltage	85 kV	100 kV
Current	71 μA	70 μA
Power	6 W	7 W
Exposure Time	4000 ms	2500 ms
Nr. of projections	3142	2500
Voxel size	4.4 μm	5.9 μm
Scanning time	310 min	105 min

Table 2
Fluid-dynamic quantities for the two electrodes: carbon felt (Sample 1) and carbon vitrified foam (Sample 2).

Quantity	*Felt*	*Foam*
Porosity ϵ	0.949	0.676
Pump Power Dens.	3500 W/m^3	3500 W/m^3
Bulk velocity U	1.42 cm/s	0.79 cm/s
Spec.Surf.Area S_s	278 cm^{-1}	545 cm^{-1}
Eff. Diff. Coeff. $\mathcal{D}_{\text{eff}}$	0.64 mm^2/s	1.00 mm^2/s
Reaction rate RR	0.28 s^{-1}	1.56 s^{-1}

In this work, two candidate materials for VRFB electrodes, namely a carbon felt and a carbon vitrified foam, are scanned by means of a metrological CT system (Nikon Metrology MCT225), characterized by micro-focus X-ray source (minimum focal spot size equal to 3 μm), 16 bit detector with 2000x2000 pixels and cabinet ensuring controlled temperature of 20 °C. The CT scanning parameters, optimized for each scanned sample, are reported in Table 1. In order to achieve high scanning resolutions, small voxel sizes are obtained (voxel means volumetric pixel) and the focal spot size is kept at a minimum by setting very low powers. A large number of bi-dimensional projections (i.e. gray-scale images representing the local attenuation of X-rays occurring when traversing the samples material) are collected at different angular positions of the scanned sample, during its rotation around the vertical axis. Three-dimensional models of the two samples are reconstructed from these projections using a filtered back-projection algorithm [20] and then aligned with respect to the flow direction in the analysis- and visualization- software VGStudio MAX 3.0 (Volume Graphics GmbH, Germany). The aligned volumes are exported into image stacks, where each gray-scale image represents a 2D cross-section of the sample orthogonal to the flow direction. The distance between consecutive sections is chosen equal to the voxel size. These images are finally used as input for flow simulations (see Section 2.2) after being binarized in Matlab (The Mathworks, USA) to discriminate between material (white) and pores (black). Note that the best resolution obtained slightly differs between the two cases, as reported in Table 1. Therefore, we have to rescale flow simulations according to the corresponding X-Ray CT voxel size.

Materials reconstruction, showed in Fig. 1, highlights the differences between the porous microstructures. The carbon felt is characterized by long and thin curved fibers, chaotically intersecting each others. On the other hand, the porous foam is characterized by a more complex structure with quasi-cylindrical pores of different size. From the structural point of view, we point out that the foam is more stiff. Such characteristic can influence the electric performance of the electrode allowing a better electric contact with the stack current collectors. For further informations about electric contact resistance in VRFB references are available in the literature, e.g [21]. Also, macroscopically, we observe no preferential orientation of fibers and pores in both materials whereas the foam presents a much higher specific surface area and a lower porosity. The values of porosity and specific surface area are reported in Fig. 3 and Table 2.

2.2. Lattice-Boltzmann method

A thorough and fruitful mathematical analysis during late 1980 s and early 1990 s revealed the exciting perspective of solving the macroscopic equations for fluid mass and momentum transport, through the Lattice-Boltzmann Method (LBM), an easy and explicit algorithm describing interaction of fluid particles built on the kinetic theory and statistical mechanics frameworks [22,23]. More recently, with the advent of parallel computing, the Lattice-Boltzmann method (LBM) gained even more attention as an alternative solution of Navier-

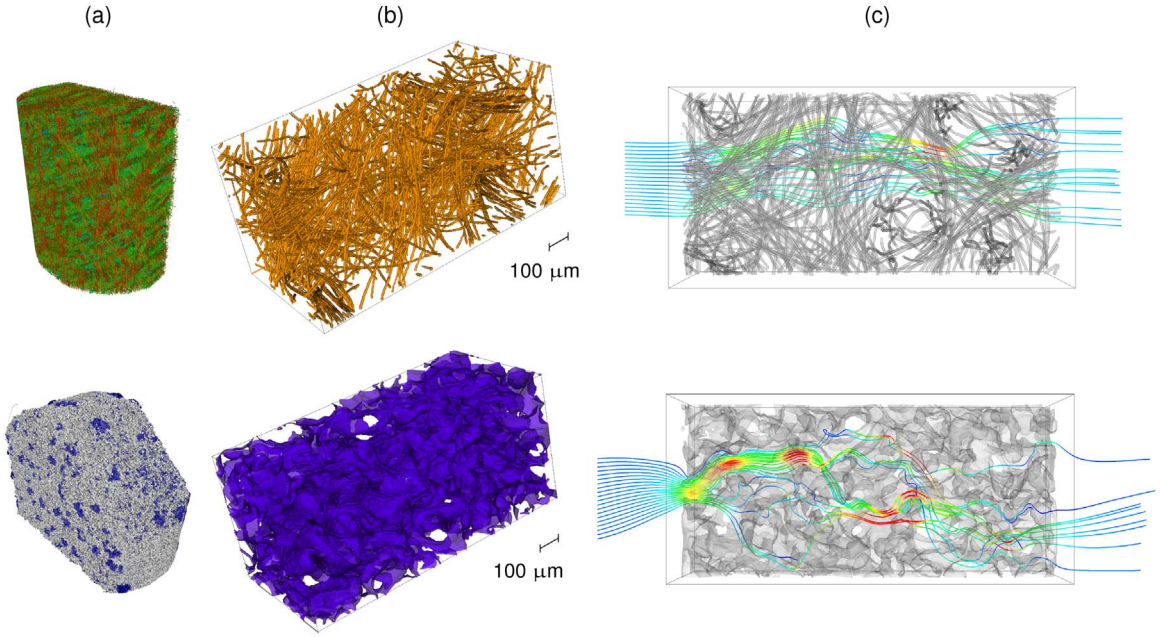

Fig. 1. Upper panels: carbon felt. Lower panels: carbon vitrified foam. (a) X-ray computed tomography reconstruction. (b) Isosurfaces of binarized volume images for the two considered samples. The corresponding binary matrices were used as geometrical input for LBM fluid flow simulations. An equivalent body force is applied along the x direction for simulating the effect of the pressure gradient. (c) Streamlines simulating reactants dispersion through the media performed by coupling LBM with LPT.

Stokes Equations because of its extreme efficiency on multi-cpu supercomputer and for its ability to handle complex geometries [24].

In this work, we use a Lattice-Boltzmann three-dimensional (D3Q19) multi-relaxation-time (MRT) model in order to solve the microscopic flow field inside the porous electrode. The capability of MRT-based LBM models of increasing the numerical accuracy in presence of complex geometries has been widely assessed [25,26]. The present numerical algorithm has been previously used in Maggiolo *et al.* [27], where validation and test cases are also presented, e.g. flows around single and packed-bed of spheres. The D3Q19 LBM solves the flow field along a regular lattice grid of interconnected computational nodes, linked by the discrete speed versors c_r along $r = 19$ directions in the three-dimensional space $i = x, y, z$. The regular structure of the computational domain is an obvious advantage for parallel computing. In the LBM-MRT framework the equation for the distribution functions reads as [28]:

$$f_r(\boldsymbol{x} + c_r\delta t, t + \delta t) - f_r(\boldsymbol{x}, t) = -\mathcal{M}^{-1}\Big\{\mathcal{S}(m_r(\boldsymbol{x}, t) - m_r^{eq}(\boldsymbol{x}, t)) - \left(\mathcal{I} - \frac{1}{2}\mathcal{S}\right)(\mathcal{M}F_r)\Big\}. \quad (1)$$

The statistics of particles, *streaming* and *collision*, is expressed by the distribution function $f_r(\boldsymbol{x}, t)$ along the r-th direction, at the position $\boldsymbol{x} = (x, y, z)$ and time t; m_r and m_r^{eq} are the set of hydrodynamic conserved and not-conserved moments and the set of equilibrium moments of distribution functions, which evolve following different relaxation times determined by the transformation matrix $\mathcal{M}$ and the collision matrix $\mathcal{S}$ ($\mathcal{I}$ is the identity matrix). [28] In order to simulate the pressure gradient $\Delta P/L$ forcing the electrolyte solution through the electrodes an equivalent body force is used following the approach proposed by Guo *et al.* [29]. The macroscopic flow fields, density ρ and momentum ρu, are then recovered from the statistical moments of the underlying fluid dynamics at the mesoscale expressed in terms of the distribution functions f_r.

Fig. 1 shows the electrode geometries used as inputs for LBM simulations. The domain length and cross sectional area are $L = 296$ and $A = 146^2$ and $L = 224$ and 108^2 computational cells, for the carbon felt and carbon vitrified foam, respectively (in metrical units $L = 1.3$ mm and $A = 0.64^2$ mm^2 for both samples). Free-slip boundary conditions were applied along both transverse directions y and z in order to simulate an infinite periodic medium. Instead, along the streamwise direction x, we impose periodic boundary condition by inserting two buffer zones at inlet and outlet and by imposing periodicity at the extremities of the whole domain. Such buffer zones are sufficiently long to allow a laminar flow rechannelling along x all over the cross sectional area A (we ensure that the buffer length is bigger than the maximum characteristic length of the flow). Simulations are performed using 24 cores in order to achieve accurate solutions in a small computational time (~ 24 h). From the LBM method we estimate the flow velocity through the porous microstructure that is used to evaluate electrolyte dispersion and reaction.

2.3. Lagrangian-Particle-Tracking

The ratio between the viscosity (momentum diffusion) and the electrolyte molecular diffusion in liquids is very high, namely around 1000. In these conditions, Eulerian techniques fail to correctly reproduce the dynamics of the electrolyte dispersion, unless using an extremely large number of mesh points to solve the thin mixing layers near the porous surfaces. A more efficient solver can be obtained using Lagrangian Particle Tracking algorithms which are able to perform simulations even in the most critical case of vanishing diffusion. They read as:

$$\dot{x}_i^p = u_i(x^p(t), y^p(t), z^p(t)) \quad (2)$$

with $\dot{x}_i^p$ the i velocity component of the tracer p and u_i the i component of the fluid velocity. Particles behave as fluid tracers following the fluid trajectories. The molecular diffusion of the tracers is then implemented using a random walk algorithm and the particle position is updated at each time step as:

$$x_i^{p,\mathcal{D}_m} = x_i^p + rnd\ \sqrt{2\mathcal{D}_m\Delta t} \quad (3)$$

where Δt is the time step, rnd a random generated number with Gaussian probability and the diffusion coefficient is set to $\mathcal{D}_m \sim 10^{-3}$ mm$^2/s$ [30]. Five thousand tracers for each medium are randomly injected in the fluid flow previously solved by the LBM algorithm, and their trajectories are followed in time according to (2). We inject tracers in the fluid phase away from the solid sample boundaries (as far as $1/8L$ along x and $1/4\sqrt{A}$ along y and z) in order to avoid nonphysical boundary effects in early dispersion regime. Solute dispersion promoted by the combined effect of pressure gradient and electrode microstructure, is then characterized by analyzing the statistics of tracers displacements in the porous medium. We compute tracer displacements by concatenating each segments of tracers trajectories inside the medium, following a similar procedure used by Kang et al. [31].

A simple model of reaction has been derived is the same framework. We assume fast chemical reactions controlled by the solute diffusion as happen in Redox Flow Battery at peak performances. Hence, the rate of electrolyte reacting at solid-fluid boundaries of the porous electrode is determined by the mass transport rate in the boundary diffusion layer which represent a thin region where mass transport and reactions occur, see Fig. 2 [32,33]. In this thin region close to solid boundary of thickness $\ell_\mu \sim O(\mu\text{m})$ [34], electrolyte particles enter by a molecular diffusion process and in the fast-chemistry limit suddenly react with a typical rate estimated by $\mathcal{D}_m/\ell_\mu^2 = 10^3$ s^{-1}. In order to mimic this process in the LPT algorithm, a particle is considered to react at fluid-solid boundary when its total displacement after the random walk step exceeds the threshold ℓ_μ, see Fig. 2. It is anticipated that different simulations with varying value of $\mathcal{D}_m$ and ℓ_μ but with the same diffusive/reaction rate $\mathcal{D}_m/\ell_\mu^2$ have been performed, leading to same results in terms of macroscopic reaction and confirming the reaction mechanism to be diffusion-dominated.

As already stated, 5000 tracers have been injected at the inlet of the electrode for estimating the global reaction rate. Tracers travel along the medium carried by the fluid flow. Once tracers reached the end of the medium, we randomly reinjected them at inlet. Finally, we determine the percentage of reacted solute n^*_{react} by averaging on equivalent intervals of time the value of the ratio between the number of reacted particles at the outlet of the medium, and the total number of particles which reached the outlet.

Being based on a fast chemistry assumption, the model quantifies the maximum global reaction rate that can be achieved in the medium. In other words, it measures the efficiency of the porous microstructure in promoting fast reactions.

3. Performance comparison

From a fluid-dynamic point of view, reaction of a solute in a electrolyte solution flowing through a porous medium is the results of

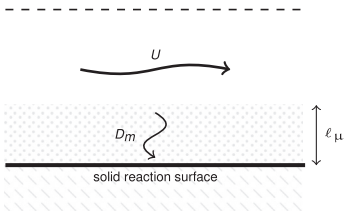

Fig. 2. Sketch of the diffusion-reaction mechanism. In the fast-chemistry limit, reaction is diffusion-controlled by the molecular mass transfer rate at fluid-solid boundary.

the complex effects of different contemporary mechanisms, as convective, diffusive e viscous actions at the pore scale. The balance between these actions determines the reaction rate and the overall current production, being the limit current density proportional to it. Since our main goal is to characterize the material efficiency induced at the microscopic scale for real-scale flow batteries applications, we extract two synthetic parameters which quantify the electrode fluid-dynamic behavior: (i) the porous effective diffusion $\mathcal{D}_{eff}$ and (ii) the reaction rate RR. Flow simulations are performed at matching pump power density $U\Delta P/L$ (where U is the mean velocity of the fluid and L the sample length at which the pressure jump ΔP is imposed) in order to consistently compare the materials fluid-mechanic performances. To this aim, all the fluid-dynamic quantities are scaled by using the voxel size length extracted from X-Ray CT electrode reconstruction (see Table 1 and 2) and the characteristic kinematic viscosity of VRFB liquid electrolytes, i.e. $\nu_e \sim 4.4\ 10^{-6}\ m^2/s$.

In VRFBs the solute should be efficiently mixed and dispersed through the porous electrode in order to attain an uniform reaction all throughout the electrode domain. The complex geometry of pores is a source for dispersion of the solute. The phenomenology behind this aspect can be seen in the (c) plots of Fig. 1. In these conditions, the effective diffusion of the electrolyte through the porous microstructure can be higher by orders of magnitude with respect to the molecular one [27], i.e. $\mathcal{D}_{eff} \gg \mathcal{D}_m$. Hence, we quantify the dispersion efficiency by computing the Mean Square Displacement MSD from the Lagrangian statistics of tracer displacements:

$$MSD(t) = \langle (dx_p - \langle dx_p \rangle)^2 + (dy_p - \langle dy_p \rangle)^2 + (dz_p - \langle dz_p \rangle)^2 \rangle \tag{4}$$

where $\langle \cdot \rangle$ indicates the average ensemble operator and $dx_p = x_p(t) - x_p(t=0)$ is the displacement of the tracer particle in the x direction (correspondent definitions hold in the other directions).

Hydrodynamic dispersion in porous media can significantly deviate from classic Fickian diffusion theory, that occurs when the Mean Square Displacement grows linearly in time [35], $MSD = 6\mathcal{D}_{eff}t$. While the mean square displacement grows with the square of time for the very first instants and then should tend to Fickian diffusion for very long times, anomalous behaviors can appear at intermediate, still long enough times [36,31,27]. With regards to electrolytes flowing through porous media where velocity is of the order of centimeters per second, the typical time scale at which dispersion expresses a strong anomalous behavior is of the order of tenths of seconds, at which fluid particles travel approximately the length of the samples herein investigated. Hence, anomalous diffusion needs to be accounted.

The inset of Fig. 3 shows the computed MSD for both samples. The global dispersion behavior is similar but the carbon foam shows higher values of the mean square displacement implying a higher effective diffusion promoted by this medium. At short times, of the order of milliseconds, the dispersion process is ballistic with $MSD \propto t^2$, as expected, whereas it grows more than linearly in time for longer distances, with $MSD \propto t^{1.3}$. This superdiffusive behavior is similar in both samples and in accordance with other data in literature for porous media transport [31,27].

Then, in order to get a global and synthetic measure of the effective dispersion promoted by the different porous microstructures, which is inherently non-linear in time, we use the method illustrated in Maggiolo *et al.* [27]: we extract an effective diffusion coefficient $\mathcal{D}_{eff}$ considering an equivalent regular diffusion process which shows the same MSD at a given macroscopic length scale, see the inset of Fig. 3. This length scale should be a characteristic size of the porous medium and here is chosen as $L_c = 1.58$ mm, i.e. the porous average length of the samples which is of the order of the electrode thickness. The effective diffusion coefficients are reported in Table 2. It appears that the effective diffusion coefficient of the carbon foam is higher than that of the felt meaning more efficient mixing process. It should be noted that present values of $\mathcal{D}_{eff} \sim$ mm$^2/s$ are much higher those estimated

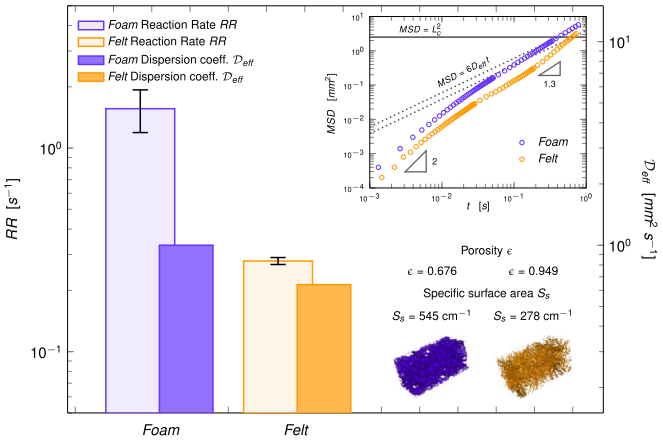

Fig. 3. Reaction rate RR (left ordinate axis) and effective dispersion coefficient $\mathcal{D}_{eff}$ (right ordinate axis) for carbon vitrified foam and carbon felt samples. Error bars indicate the standard error computed by varying the sample length L. Inset: mean square displacement MSD against time for both samples; the effective dispersion coefficient $\mathcal{D}_{eff}$ had been determined from the equivalent Fickian process corresponding to dispersion at the electrode length L. On the bottom-right corner are reported the values of porosity ϵ and specific surface area S_s.

using the Bruggeman correction [8] $\mathcal{D}_{eff,\,Br.} = \epsilon^{3/2}\mathcal{D}_m$ (ϵ the porosity) that are of the order of 10^{-3} mm^2/s. Actually, the Bruggeman correction accounts for the effects of the porous medium on a regular diffusion process without convection. While it is expected to work well for gases where the molecular diffusion coefficients are relatively high ~10 mm^2/s and $\mathcal{D}_{eff,\,Br.}$ are of similar order magnitude, the situation changes for liquids where the molecular diffusion coefficients are much lower (as in present cases) and the effective diffusion is dominated by the flow transport through the pores. In addition we note that the Bruggeman corrected diffusion coefficient of the felt, $\mathcal{D}_{eff,\,Br.} = 0.93\ 10^{-3}$ mm^2/s, is higher than that of foam, $\mathcal{D}_{eff,\,Br.} = 0.55\ 10^{-3}$ mm^2/s. This is the opposite behavior with respect to the present findings based on the microscopic analysis, see Table 2. More details on the modeling of the effective diffusion for liquids in porous electrodes can be found in [27].

While dispersion is a measure of the electrode capability of solute transport and mixing, the global reaction rate measures the overall velocity of electrochemical reaction which in turn is influenced by the mixing and by the active surface area. We quantify the reaction rate RR from the mass flow rate of reacting tracers ρUA at inlet and outlet. Bearing in mind that the bulk velocity U and the cross section areas at inlet and outlet are equal, A, and denoting the medium volume as $Vol = AL$, the reaction rate is determined as:

$$RR = \frac{(\rho_{in} - \rho_{out})UA}{\rho_{in} Vol} = \frac{n^*_{react}}{L}U \tag{5}$$

where $n^*_{react} = 1 - \rho_{out}/\rho_{in}$ is the percentage of solute tracers reacting in an electrode of length L ($\rho_{in/out}$ is the reactant concentration in the inlet and outlet section, respectively). We note that n^*_{react} scales with L as expected from a dimensional analysis and as confirmed by different numerical simulations performed with different values of L (not shown here). The data we will show fix $L = 1.3\ mm$ as the length of the samples.

In the fast-chemistry limit, the reaction rate computed in the carbon vitrified foam is more than five times higher than the one computed in the carbon felt, as well depicted in Fig. 3 and reported in Table 2. This significant improvement can be ascribed to the inherently different nature of the foam material microstructure in comparison with the fibrous felt one. In particular, (i) to the higher tortuosity of fluid paths which enhances the effective reactant dispersion (as well highlighted in Fig. 1 and measured in Fig. 3) and (ii) to the higher amount of fluid-solid surface available for electrochemical reaction which is almost the double for the foam, see the specific surface areas, S_s, reported in Table 2.

4. Final remarks

We propose a new methodology to test the fluid-mechanic efficiency of innovative materials for porous electrodes of Vanadium Redox Flow Batteries. This methodology uses state-of-the-art numerical and metrological techniques: fluid-dynamics simulations using the Lattice-Boltzmann-Method to evolve the flow in complex geometries at the pore-scale, a Lagrangian-Particle-Tracking to evolve solutes with very low molecular diffusions and a X-ray Computed-Tomography to extract the real electrode porous media geometry at pore-scale. The method allows to identify the capacity of the porous electrode in mixing the electrolyte and in promoting the reactions at the pore-scale level. We applied this technique at two different real samples of porous electrodes with very different microstructures: a vitrified carbon foam with porosity $\epsilon = 0.676$ and a fibrous carbon felt with porosity $\epsilon = 0.949$. From the present microscopic analysis we find that carbon foam shows both higher capacity in mixing electrolytes and in promoting the global reaction rate. The combined effect of the higher tortuosity (effective diffusivity) and of specific surface area of this sample promotes reactions.

By using this methodology it will be possible to test different materials for electrodes and understand the guidelines to design original porous electrodes for Vanadium Redox Flow Batteries starting from the microscopic pore-scale features. Innovative electrode materials will be then also tested in an industrial-scale stack in order to experiment their overall performances in real industrial conditions. Their performance will be compared with that obtained for thick carbon felt electrodes assembled into a 600 cm^2 40 cell stack, where current density in excess of 380 A (i.e. 635 mA/cm^2) have been recently measured.

Acknowledgements

This work was funded by the University of Padova under the strategic project MAESTRA 2011 “From Materials for Membrane-Electrode Assemblies to Electric Energy Conversion and Storage Device” (cod. STPD11XNRY_002).

References

[1] Doe global energy storage database, ⟨www.energystorageexchange.org⟩.
[2] G. Crabtree, The joint center for energy storage research: A new paradigm for battery research and development, in: AIP Conference Proceedings, vol. 1652, AIP, 2015, pp. 112–128. http://dx.doi.org/10.1063/1.4916174.
[3] B. Sun, M. Skyllas-Kazacos, Chemical modification of graphite electrode materials for vanadium redox flow battery applicationpart ii. acid treatments, Electrochim. Acta 37 (13) (1992) 2459–2465. http://dx.doi.org/10.1016/0013-4686(92)87084-D.
[4] D. Aaron, Q. Liu, Z. Tang, G. Grim, A. Papandrew, A. Turhan, T. Zawodzinski, M. Mench, Dramatic performance gains in vanadium redox flow batteries through modified cell architecture, J. Power Sources 206 (2012) 450–453. http://dx.doi.org/10.1016/j.jpowsour.2011.12.026.
[5] Q. Zheng, F. Xing, X. Li, G. Ning, H. Zhang, Flow field design and optimization based on the mass transport polarization regulation in a flow-through type vanadium flow battery, J. Power Sources 324 (2016) 402–411. http://dx.doi.org/10.1016/j.jpowsour.2016.05.110.
[6] T.J. Latha, S. Jayanti, Ex-situ experimental studies on serpentine flow field design for redox flow battery systems, J. Power Sources 248 (2014) 140–146. http://dx.doi.org/10.1016/j.jpowsour.2013.09.084.
[7] S. Kumar, S. Jayanti, Effect of flow field on the performance of an all-vanadium redox flow battery, J. Power Sources 307 (2016) 782–787. http://dx.doi.org/10.1016/j.jpowsour.2016.01.048.
[8] V.D. Bruggeman, Berechnung verschiedener physikalischer konstanten von heterogenen substanzen. i. dielektrizitätskonstanten und leitfähigkeiten der mischkörper aus isotropen substanzen, Ann. Phys. 416 (7) (1935) 636–664. http://dx.doi.org/10.1002/andp.19354160705.
[9] G. Qiu, A.S. Joshi, C. Dennison, K. Knehr, E. Kumbur, Y. Sun, 3-d pore-scale resolved model for coupled species/charge/fluid transport in a vanadium redox flow battery, Electrochim. Acta 64 (2012) 46–64. http://dx.doi.org/10.1016/j.electacta.2011.12.065.
[10] G. Qiu, C. Dennison, K. Knehr, E. Kumbur, Y. Sun, Pore-scale analysis of effects of electrode morphology and electrolyte flow conditions on performance of vanadium redox flow batteries, J. Power Sources 219 (2012) 223–234. http://dx.doi.org/10.1016/j.jpowsour.2012.07.042.
[11] P. Trogadas, O.O. Taiwo, B. Tjaden, T.P. Neville, S. Yun, J. Parrondo, V. Ramani, M.-O. Coppens, D.J. Brett, P.R. Shearing, X-ray micro-tomography as a diagnostic tool for the electrode degradation in vanadium redox flow batteries, Electrochem. Commun. 48 (2014) 155–159. http://dx.doi.org/10.1016/j.elecom.2014.09.010.
[12] R. Jervis, L.D. Brown, T.P. Neville, J. Millichamp, D.P. Finegan, T.M. Heenan, D.J. Brett, P.R. Shearing, Design of a miniature flow cell for in situ x-ray imaging of redox flow batteries, J. Phys. D: Appl. Phys. 49 (43) (2016) 434002. http://dx.doi.org/10.1088/0022-3727/49/43/434002.
[13] G. Hu, M. Jing, D.-W. Wang, Z. Sun, C. Xu, W. Ren, H.-M. Cheng, C. Yan, X. Fan, F. Li, A gradient bi-functional graphene-based modified electrode for vanadium redox flow batteries, Energy Storage Mater. 13 (2018) 66–71.
[14] W.W. Wits, S. Carmignato, F. Zanini, T. Vaneker, Porosity testing methods for the quality assessment of selective laser melted parts, CIRP Ann. Manuf. Technol. 65 (1) (2016) 201–204. http://dx.doi.org/10.1016/j.cirp.2016.04.054.
[15] L.Y., S. Lee, J. Youn, K. Chung, T. Kang, Characterization of fiber orientation in short fiber reinforced composites with an image processing technique, Material Research Innovation 6 (2002) 65–72. http://dx.doi.org/10.1007/s10019-002-0180-8.
[16] S. Khademzadeh, S. Carmignato, N. Parvin, F. Zanini, P.F. Bariani, Micro porosity analysis in additive manufactured niti parts using micro computed tomography and electron microscopy, Mater. Des. 90 (2016) 745–752.
[17] P. Hermanek, S. Carmignato, Reference object for evaluating the accuracy of porosity measurements by x-ray computed tomography, Case Stud. Nondestruct. Test. Eval. 6 (2016) 122–127.
[18] L. De Chiffre, S. Carmignato, J.P. Kruth, R. Schmitt, A. Weckenmann, Industrial applications of computed tomography, CIRP Ann. - Manuf. Technol. 63 (2014) 655–667. http://dx.doi.org/10.1016/j.cirp.2014.05.011.
[19] J.P. Kruth, M. Bartscher, S. Carmignato, R. Schmitt, L. De Chire, A. Weckenmann, Computed tomography for dimensional metrology. cirp annals - manufacturing technology, CIRP Ann. - Manuf. Technol. 60 (2) (2011) 821–842. http://dx.doi.org/10.1016/j.cirp.2011.05.006.
[20] L.A. Feldkamp, L.C. Davis, J.W. Kress, Practical cone-beam algorithm, J. Opt. Soc. Am. 1 (6) (1984) 612–619.
[21] S.-K. Park, J. Shim, J.H. Yang, C.-S. Jin, B.S. Lee, Y.-S. Lee, K.-H. Shin, J.-D. Jeon, The influence of compressed carbon felt electrodes on the performance of a vanadium redox flow battery, Electrochim. Acta 116 (2014) 447–452.
[22] U. Frisch, B. Hasslacher, Y. Pomeau, Lattice-gas automata for the navier-stokes equation, Phys. Rev. Lett. 56 (14) (1986) 1505. http://dx.doi.org/10.1103/PhysRevLett.56.1505.
[23] G. McNamara, B. Alder, Analysis of the lattice boltzmann treatment of hydrodynamics, Phys. A: Stat. Mech. its Appl. 194 (1) (1993) 218–228. http://dx.doi.org/10.1016/0378-4371(93)90356-9.
[24] S. Succi, The Lattice Boltzmann Equation: For Fluid Dynamics and Beyond, Oxford University Press, 2001.
[25] P. Lallemand, L.-S. Luo, Theory of the lattice boltzmann method: dispersion, dissipation, isotropy, galilean invariance, and stability, Phys. Rev. E 61 (6) (2000) 6546. http://dx.doi.org/10.1103/PhysRevE.61.6546.
[26] D. dHumières, I. Ginzburg, Viscosity independent numerical errors for lattice boltzmann models: from recurrence equations to magic collision numbers, Comput. Math. Appl. 58 (5) (2009) 823–840. http://dx.doi.org/10.1016/j.camwa.2009.02.008.
[27] D. Maggiolo, F. Picano, M. Guarnieri, Flow and dispersion in anisotropic porous media: A lattice-boltzmann study, Physics of Fluids 28 (102001). http://dx.doi.org/10.1063/1.4963766.
[28] D. d'Humières, Multiple-relaxation-time lattice boltzmann models in three dimensions, Philos. Trans. R. Soc. Lond. A: Math. Phys. Eng. Sci. 360 (1792) (2002) 437–451. http://dx.doi.org/10.1098/rsta.2001.0955.
[29] Z. Guo, C. Zheng, B. Shi, Discrete lattice effects on the forcing term in the lattice boltzmann method, Phys. Rev. E 65 (4) (2002) 046308. http://dx.doi.org/10.1103/PhysRevE.65.046308.
[30] Z. Jiang, K. Klyukin, V. Alexandrov, Structure, hydrolysis, and diffusion of aqueous vanadium ions from car-parrinello molecular dynamics, J. Chem. Phys. 145 (11) (2016) 114303.
[31] P.K. Kang, P. Anna, J.P. Nunes, B. Bijeljic, M.J. Blunt, R. Juanes, Pore-scale intermittent velocity structure underpinning anomalous transport through 3-d porous media, Geophys. Res. Lett. 41 (17) (2014) 6184–6190. http://dx.doi.org/10.1002/2014GL061475.
[32] R.B. Bird, W.E. Stewart, L.E.N., Transport Phenomena, Wiley, 2007.
[33] Y.A. Gandomi, D. Aaron, T. Zawodzinski, M. Mench, In situ potential distribution measurement and validated model for all-vanadium redox flow battery, J. Electrochem. Soc. 163 (1) (2016) A5188–A5201.
[34] B. Levich, The theory of concentration polarisation, Discuss. Faraday Soc. 1 (1947) 37–49.
[35] B. Wang, J. Kuo, S.C. Bae, S. Granick, When brownian diffusion is not Gaussian, Nat. Mater. 11 (6) (2012) 481–485. http://dx.doi.org/10.1038/nmat3308.
[36] P. De Anna, T. Le Borgne, M. Dentz, A.M. Tartakovsky, D. Bolster, P. Davy, Flow intermittency, dispersion, and correlated continuous time random walks in porous media, Phys. Rev. Lett. 110 (18) (2013) 184502. http://dx.doi.org/10.1103/PhysRevLett.110.184502.